SAND2020-0556C

Large-Scale Battery Energy Storage System Dynamic Model for Power System Stability Analysis

Roghieh A. Biroon (rabdoll@clemson.edu), *Student Member, IEEE,* Pierluigi Pisu (pisup@clemson.edu), *Member,* IEEE and David Schoenwald (daschoe@sandia.gov), *Senior Member, IEEE*

***Abstract*—The increasing penetration of renewable energy sources in the grid can raise the likelihood of instability in the power grid, e.g. small signal and voltage instability incidents. To study the effect of BESS integration on the grid and power system behavior, accurate battery modeling plays a key role. As the majority of power system studies including small signal stability analysis is carried out in the *d-q* axes, a precise model of the battery in the *d-q* axes is necessary. The lack of parametric based models of the battery in *d-q* axes makes stability analysis more challenging especially as the contributions of batteries in power systems are growing rapidly. In this paper, we develop an analytical model for the battery and its inverter in *d-q* axes. To validate the fidelity of the model, we simulate both the original and the obtained *d-q* models and compare the simulation results.**

***Index Terms*-- Battery energy storage system, disturbance rejection, load frequency control, small signal stability.**

I. Introduction

The growing interest of battery energy storage systems (BESSs) in power grids highlights their significant role in future power grids. At the transmission level of power grids, large-scale batteries can provide load frequency control due to their fast response. Battery integration in the power grid can effectively reduce oscillations in frequency and tie-line power profiles caused by small load disturbances [1]. In general, small time constants, fast response, and their high energy density creates a large spectrum of potential applications for BESSs in power systems.

There exists considerable literature on different applications of BESSs in power systems. The effects of batteries incorporating AGC on the load frequency regulations have been studied in [2] - [3]. Moreover, batteries as backups for microgrids and large wind farms are studied in [4] and [5]. In [4], it is shown that a large-scale battery energy storage in an isolated microgrid can improve the microgrid dynamic performance in response to the power system dynamics. In [5], the effects of battery integration in a wind farm is studied from the power system stability and control point of view. Moreover, battery integration in the power system can improve the spectral response of a large wind-integrated power system and damp the system's frequency oscillations. In [6], coordinated controllers for a wind farm and a BESS in charging mode are designed to guarantee the nearly perfect matching of the grid spectral response to a desired response. Large scale battery integration in the power system also improves the transient stability of the power system. In [7], battery integration in the power system enhances the transient stability during the active power transferring process through transmission lines. In [7], it is also shown that the transient stability performance of the system is enhanced by suitable placement of a BESS in the system. To analyze the effects of BESSs in power grids for all the aforementioned applications, a precise model is required.

The dynamic model for large-scale batteries and their integration in power grids was first proposed in [8]. In this model, the battery was represented by a constant voltage source parallel to a resistance and capacitor (RC) circuit. The model was later improved and implemented in power system studies [9]-[10]. The proposed model in [10] has been used in research studies for load frequency control and power system stability analysis [6], [7], [11]. However, nonlinearity is the major disadvantage of the battery model in [10] as it complicates the stability analysis. Moreover, in the majority of the existing literature, BESS is studied as additional active power source from real power and frequency variation points of views, while the major advantage of BESS is the fact that both its active power and power factor are adjustable and controllable by the firing angle of the thyristors in the inverter. Therefore, by controlling the inverter, it is possible to have reactive power injection in the power system. As the reactive power directly affects the voltage deviation in power systems, unstudied reactive power flow may cause voltage instability in the network. Hence, in power systems small signal stability analysis, *d-q* models of power system components in state space representation must be developed.

This paper describes a new modeling approach using *d-q* analysis for batteries integrated with the power grid. A state space representation of the battery energy storage model accompanied by an inverter in the *d-q* axes is presented. The inverter firing angle is considered as an input enabling the control the battery's power factor

The advantages of the proposed model with respect to the other battery models [6] – [7] and [11] are: *i)* the reactive power has been considered such that grid voltage deviations can be taken into account. and *ii)* the state space model of the battery has been represented in *d-q* structure, which utilize the stability analysis in the power system.

The rest of the paper is organized as follows. Section II describes the problem statement. In Section III, the battery equations and linearized model in the *d-q* axes are presented. Simulation results are shown in Section IV. Finally, Section V presents conclusions and future study.

978-1-7281-4436-8/20/$31.00 ©2020 IEEE

Sandia National Laboratories is a multimission laboratory managed and operated by National Technology & Engineering Solutions of Sandia, LLC, a wholly owned subsidiary of Honeywell International Inc., for the U.S. Department of Energy's National Nuclear Security Administration under contract DE-NA0003525.

II. PROBLEM STATEMENT

Small signal stability in a power system is defined as the ability of the power system to maintain synchronism in the presence of small disturbances such as load deviations. In this context, since the power system is inherently a nonlinear system, the power system model is linearized in the vicinity of its operating point for the small signal analysis. This enables us to apply linear system theory to the power system even though the system is inherently nonlinear. In this regard, all power system components can be modeled in the state space representation as

$$\begin{cases} \dot{x} = Ax + Bu \\ y = Cx + Du \end{cases} \tag{1}$$

A general power system structure is shown in Fig. 1. Based on the given model, we can define the general equation of the system as:

$$[Y_{bus}]\Delta v_t = \Delta I_G - \Delta I_L - \Delta I_S + \Delta I_B \tag{2}$$

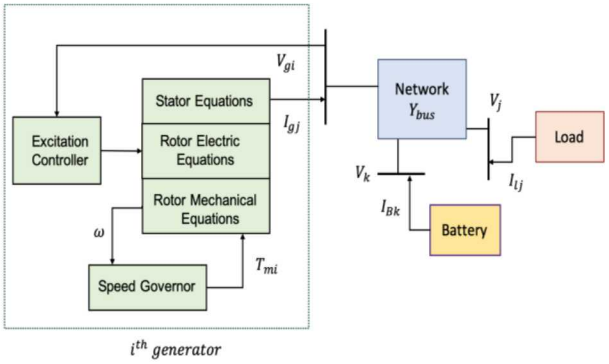

Fig. 1. Power system Structure

where, Y_{bus} is the power system admittance matrix, Δv_t is the voltage deviation in the buses and $\Delta I_G, \Delta I_L, \Delta I_S,$ and ΔI_B are the changes in generator, load, static var compensator (SVC) and battery current injections to the power system, respectively.

A. Generator Model

The generator model in state space representation varies based on the modeling approaches chosen [12]– [13]. For instance, in [12] the generator is represented with five states as:

$\Delta x_g = [\Delta\delta, \Delta\omega, \Delta E'_d, \Delta E'_q, \Delta E_{fd}]$

where, δ is rotor angle, ω is the rotational speed, $\Delta E'_d$ and $\Delta E'_q$ are the d and q axes generator internal voltages and ΔE_{fd} is the field voltage. The order of the generator model can increase to 16 states as the generator model includes the exciter, power system stabilizer (PSS), and turbine dynamics. The generator differential equations after linearization are:

$$\begin{cases} \Delta\dot{x}_g = [A_g]\Delta x_g + [B_g]\Delta V_g + [E_g]\Delta u_{cg} \\ \Delta I_g = [C_g]\Delta x_g + [D_g]\Delta V_g \end{cases} \tag{3}$$

where ΔV_g represents the voltage deviation in the generator bus, ΔI_g is the generator current deviation and Δu_{cg} is a small perturbation in the generator reference input variables for the generator controllers. Note that, ΔI_g, and ΔV_g are represented in d-q axes as

$$\Delta I_g = \begin{bmatrix} \Delta I_{dg} \\ \Delta I_{qg} \end{bmatrix} \text{ and } \Delta V_g = \begin{bmatrix} \Delta V_{qg} \\ \Delta V_{dg} \end{bmatrix}$$

To be able to study the power system, all other equipment such as loads, SVCs and batteries should be written in $d-q$ format. These devices are modeled in state space representation in the following subsections.

B. Load model

Power system loads including induction motors and nonlinear loads are modeled as

$$\begin{cases} \Delta\dot{x}_l = [A_l]\Delta x_l + [B_l]\Delta V_l + [E_l]\Delta u_{cl} \\ \Delta I_l = [C_l]\Delta x_l + [D_l]\Delta V_l \end{cases} \tag{4}$$

where, Δx_l are the dynamic loads such as induction motor states and Δu_{cl} are the load control inputs. ΔV_l is the load bus voltage deviation and ΔI_l is the load (demand) current deviation. For the static loads the equation will be simplified to

$$\Delta I_l = [D_l]\Delta V_l = [Y_l]\Delta V_l \tag{5}$$

C. SVC model

Similar to the load equations, static *var* compensator (SVC) in state space representation is modeled as

$$\begin{cases} \Delta\dot{x}_s = [A_s]\Delta x_s + [B_s]\Delta V_s + [E_s]\Delta u_{cs} \\ \Delta I_s = [C_s]\Delta x_s + [D_s]\Delta V_s \end{cases} \tag{6}$$

where, Δx_s are the SVC states and Δu_{cs} are the SVC control inputs. ΔV_s and ΔI_s are the SVC bus voltage and current deviations, respectively.

D. Battery model

To add the battery dynamics to the power system model, the battery also should be represented as

$$\begin{aligned} \Delta\dot{x}_b &= [A_b]\Delta x_b + [B_b]\Delta V_b + [E_b]\Delta u_{cb} \\ \Delta I_b &= [C_b]\Delta x_b + [D_b]\Delta V_b \end{aligned} \tag{7}$$

Remark1: Note that all equations are in d-q axes, hence:

$$\Delta I_{(.)} = \begin{bmatrix} \Delta I_d \\ \Delta I_q \end{bmatrix} \text{ and } \Delta V_{(.)} = \begin{bmatrix} \Delta v_q \\ \Delta v_d \end{bmatrix} \tag{8}$$

where $\Delta V_{(.)}$ represents voltages deviations in load, SVC or the battery buses, $\Delta I_{(.)}$ is the current deviations and $\Delta u_{c(.)}$ is the small perturbation in their reference input variables.

E. Network Equations

As shown in Fig. 1, generators and loads in the power system network are interfaced to the network as current injections This leads us to following equation

$$[Y_{bus\_DQ}]\Delta V_{QD} = [P_G]\Delta I_G - [P_L]\Delta I_L - [P_L]\Delta I_S + [P_B]\Delta I_B \tag{9}$$

Y_{bus_DQ} is the network admittance matrix in d-q axes and $P_g(i,j) = \begin{bmatrix} 1 & 0 \\ 0 & 1 \end{bmatrix}$ if the i_{th} generator is connected to the j_{th}

bus, otherwise $P_g(i,j) = \begin{bmatrix} 0 & 0 \\ 0 & 0 \end{bmatrix}$. Same interfacing matrices are defined for P_l, P_{svc}, and P_B [12]-[13].

After substituting the equations (3), (4), (5), and (7) in (9) and simplifying, the overall system representation becomes

$$\dot{X} = [A_t]X + [E]U_c \tag{10}$$

where

$$A_t = [A] + [B][P]^t[Y'_{bus_{DQ}}]^{-1}[P][C] \tag{11}$$

$$[P] = [P_G\ P_L\ P_S\ P_B] \tag{12}$$

And

$$\left[Y'_{bus_{DQ}}\right]\Delta V_{QD} = [P_G][C_G][X_G] + [P_L][C_L][X_L] + [P_S][C_S][X_S] + [P_B][C_B][X_B] \tag{13}$$

A_t represents the state matrix of the entire power grid, and the stability of the system is studied based on A_t.

To be able to study the effect of the battery integration on the power system stability, we need to model the battery in the state space model structure given in (7). Then we will be able to add the battery model to the power system model in (9). For this purpose, we derive the BESS current equations in *d-q* axes and linearize them in the vicinity of the operating point.

III. Battery Model

Large-scale batteries are accompanied by their inverters in power grids [10]. Figure 2 shows the equivalent circuit model of a battery and its inverter. To extract the state space model of the battery, we consider two cases for the charging and discharging modes. The dynamics of the battery in the charging mode are slightly different from the discharging model. In the first case, we obtain the state space model of the battery for the charging scenario. In the second case, with slight modifications, we obtain the discharging model from the first case.

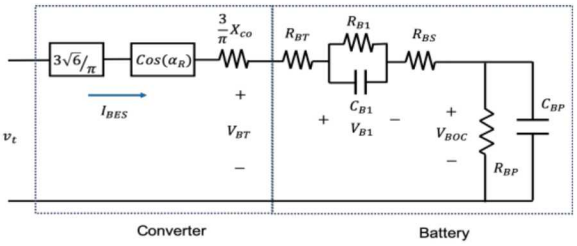

Fig. 2. Battery and inverter circuit model

A. Case I: Charging Mode

In the charging mode, using Kirchhoff's voltage law, the output voltage of the battery, V_{BT}, is

$$V_{BT} = \frac{3\sqrt{6}}{\pi} v_t\, cos(\alpha_R) - \frac{3}{\pi} x_{co} I_{BES} \tag{14}$$

where, I_{BES} is the battery's terminal current. The dynamic model of the battery for the charging mode is shown in Fig. 3, where, α_R is the inverter firing angle and v_t is the bus voltage to which the battery is connected.

Defining $\lambda = 1 + \frac{3}{\pi R} x_{co}$, and $\mathrm{R} = \mathrm{R_{BS}} + \mathrm{R_{BT}}$ the battery current is

$$I_{BES} = \frac{3\sqrt{6}}{\pi\lambda R} v_t\, cos(\alpha_R) - \frac{1}{\lambda R} V_{BOC} - \frac{1}{\lambda R} V_{B1} \tag{15}$$

where V_{B1} is the battery overvoltage, and V_{BOC} is the battery open circuit voltage. In the nonlinear model of the battery represented in Fig. 3, we consider $x_b = [V_{BOC}, V_{Bq}, \alpha_R]^T$ as the state vector of the battery.

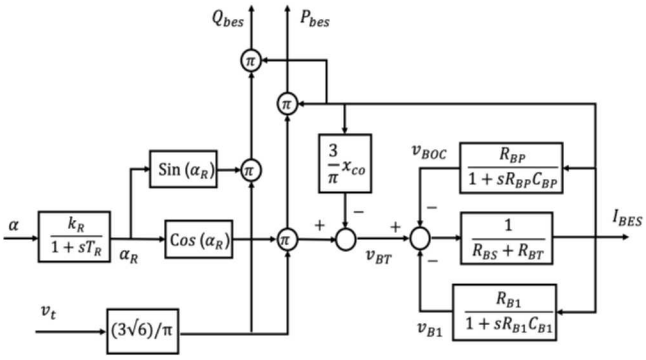

Fig. 3. Battery and inverter dynamic model in the charging mode

By linearizing (15) in the vicinity of the operating point of $\alpha_R = \alpha_{r0}$, $v_t = v_{t0}$, $V_{BOC} = V_{boc0}$, $V_{B1} = V_{b10}$, and $I_{BES} = I_{b0}$, the current deviation is

$$\Delta I_{BES} = \frac{3\sqrt{6}}{\pi\lambda R} cos(\alpha_{r0})\, \Delta v_t - \frac{3\sqrt{6}}{\pi\lambda R} v_{t0}\, sin(\alpha_{r0})\, \Delta\alpha_R - \frac{1}{\lambda R}\Delta V_{BOC} - \frac{1}{\lambda R}\Delta V_{B1} \tag{16}$$

Moreover, using the dynamic block diagram shown in Fig. 3, we have the following state dynamics

$$\Delta\dot{V}_{BOC} = \frac{1}{C_{BP}}\Delta I_{BES} - \frac{1}{C_{BP}R_{BP}}\Delta V_{BOC} \tag{17}$$

$$\Delta\dot{V}_{B1} = \frac{1}{C_{B1}}\Delta I_{BES} - \frac{1}{C_{B1}R_{B1}}\Delta V_{B1} \tag{18}$$

$$\Delta\dot{\alpha}_R = \frac{k_R}{T_R}\Delta\alpha - \frac{1}{T_R}\Delta\alpha_R \tag{19}$$

Now, considering

$$P_{BES} = \frac{3\sqrt{6}}{\pi} v_t\, I_{BES}\, cos\,(\alpha_R) \tag{20}$$

$$Q_{BES} = \frac{3\sqrt{6}}{\pi} v_t\, I_{BES}\, sin\,(\alpha_R) \tag{21}$$

$$I_{bd} = \frac{v_{td}P_{BES} - v_{tq}Q_{BES}}{v_t^2} \tag{22}$$

$$I_{bq} = \frac{v_{tq}P_{BES} + v_{td}Q_{BES}}{v_t^2} \tag{23}$$

$$v_t = \sqrt{v_d^2 + v_q^2} \tag{24}$$

The final state space representation of the battery dynamics and its inverter can be summarized as (25)-(26) in the vicinity of its operating point. In this state space model, the states are the deviation values of nonlinear states as $\Delta x_b = [\Delta V_{BOC}, \Delta V_{Bq}, \Delta\alpha_R]^T$. The input reference control for the battery is defined as $\Delta u_{cb} = \Delta\alpha$, which controls the active and reactive output power of the battery. The outputs are active (ΔI_{bd}) and reactive (ΔI_{bq}) current deviations of the battery. Note that the voltage input signal is in *d-q* axes as $\Delta v =$

$[\Delta v_q, \Delta v_d]^T$. Note that Δv is the battery terminal voltage deviation as a result of the battery connection to the power grid.

$$\begin{bmatrix} \Delta \dot{V}_{BOC} \\ \Delta \dot{V}_{B1} \\ \Delta \dot{\alpha}_R \end{bmatrix} = A_b \begin{bmatrix} \Delta V_{BOC} \\ \Delta V_{B1} \\ \Delta \alpha_R \end{bmatrix} + B_b \, \Delta v + E_b \Delta u_{cb} \tag{25}$$

$$\begin{bmatrix} \Delta I_{bd} \\ \Delta I_{bq} \end{bmatrix} = C_b \begin{bmatrix} \Delta V_{BOC} \\ \Delta V_{B1} \\ \Delta \alpha_R \end{bmatrix} + D_b \, \Delta v \tag{26}$$

where

$$A_b = \begin{bmatrix} \left(\frac{-1}{R_{BP}C_{BP}} - \frac{1}{R\lambda C_{BP}}\right) & \frac{-1}{R\lambda C_{BP}} & \frac{-3\sqrt{6}.v_{t0}}{\pi R\lambda C_{BP}} \sin(\alpha_{r0}) \\ \frac{-1}{R\lambda C_{B1}} & \left(\frac{-1}{R_{B1}C_{B1}} - \frac{1}{R\lambda C_{B1}}\right) & \frac{-3\sqrt{6}.v_{t0}}{\pi R\lambda C_{B1}} \sin(\alpha_{r0}) \\ 0 & 0 & \frac{-1}{T_R} \end{bmatrix} \tag{27}$$

$$B_b = \begin{bmatrix} \frac{3\sqrt{6}\, v_{q0}}{\pi\lambda C_{BP} v_{t0}} \cos(\alpha_{r0}) & \frac{3\sqrt{6}\, v_{d0}}{\pi\lambda C_{BP} v_{t0}} \cos(\alpha_{r0}) \\ \frac{3\sqrt{6}\, v_{q0}}{\pi R\lambda C_{B1} v_{t0}} \cos(\alpha_{r0}) & \frac{3\sqrt{6}.v_{d0}}{\pi R\lambda C_{B1} v_{t0}} \cos(\alpha_{r0}) \\ 0 & 0 \end{bmatrix} \tag{28}$$

$$E_b = \begin{bmatrix} 0 \\ 0 \\ \frac{k_R}{T_R} \end{bmatrix} \tag{29}$$

Finally, the terms of $C_b = [C_{bij}]$ and $D_b = [D_{bij}]$ matrices (ij representing the i^{th} and j^{th} columns) are as follows

$$C_{b11} = \frac{-3\sqrt{6}\, v_{d0}}{\pi R\lambda v_{t0}} cos(\alpha_{r0}) + \frac{3\sqrt{6}\, v_{q0}}{\pi R\lambda v_{t0}} sin(\alpha_{r0}) \tag{30}$$

$$C_{b12} = \frac{-3\sqrt{6}\, v_{d0}}{\pi R\lambda v_{t0}} cos(\alpha_{r0}) + \frac{3\sqrt{6}\, v_{q0}}{\pi R\lambda v_{t0}} sin(\alpha_{r0}) \tag{31}$$

$$C_{b13} = \frac{-54}{\pi^2 R\lambda} v_{d0}.sin(2\alpha_{r0}) - \frac{54}{\pi^2 R\lambda} v_{q0}.cos(2\alpha_{r0}) + \frac{3\sqrt{6}}{\pi R\lambda v_{t0}} (V_{boc0} + V_{b10})[v_{d0}.sin(\alpha_{r0}) + v_{q0}.cos(\alpha_{r0})] \tag{32}$$

$$C_{b21} = \frac{-3\sqrt{6}\, v_{q0}}{\pi R\lambda v_{t0}} cos(\alpha_{r0}) - \frac{3\sqrt{6}\, v_{d0}}{\pi R\lambda v_{t0}} sin(\alpha_{r0}) \tag{33}$$

$$C_{b22} = \frac{-3\sqrt{6}\, v_{q0}}{\pi R\lambda v_{t0}} cos(\alpha_{r0}) - \frac{3\sqrt{6}\, v_{d0}}{\pi R\lambda v_{t0}} sin(\alpha_{r0}) \tag{34}$$

$$C_{b23} = \frac{54}{\pi^2 R\lambda} v_{d0}.cos(2\alpha_{r0}) - \frac{54}{\pi^2 R\lambda} v_{q0}.sin(2\alpha_{r0}) + \frac{3\sqrt{6}}{\pi R\lambda v_{t0}} (V_{boc0} + V_{b10})[v_{q0}.sin(\alpha_{r0}) - v_{d0}.cos(\alpha_{r0})] \tag{35}$$

and

$$D_{b11} = \frac{-27}{\pi^2 R\lambda} sin(2\alpha_{r0}) + \frac{3\sqrt{6}}{\pi R\lambda v_{t0}^3} [v_{d0}^2 \, sin(\alpha_{r0}) + v_{d0} v_{q0} cos(\alpha_{r0})](V_{boc0} + V_{b10}) \tag{36}$$

$$D_{b12} = \frac{54}{\pi^2 R\lambda} cos^2(\alpha_{r0}) - \frac{3\sqrt{6}}{\pi R\lambda v_{t0}^3} [v_{q0}^2 \, cos(\alpha_{r0}) + v_{d0} v_{q0} sin(\alpha_{r0})](V_{boc0} + V_{b10}) \tag{37}$$

$$D_{b21} = \frac{54}{\pi^2 R\lambda} cos^2(\alpha_{r0}) - \frac{3\sqrt{6}}{\pi R\lambda v_{t0}^3} [v_{d0}^2 \, cos(\alpha_{r0}) - v_{d0} v_{q0} \, sin(\alpha_{r0})](V_{boc0} + V_{b10}) \tag{38}$$

$$D_{b22} = \frac{27}{\pi^2 R\lambda} sin(2\alpha_{r0}) - \frac{3\sqrt{6}}{\pi R\lambda v_{t0}^3} [v_{q0}^2 sin(\alpha_{r0}) - v_{d0} v_{q0} \, cos(\alpha_{r0})](V_{boc0} + V_{b10}) \tag{39}$$

Having derived the state space model for the battery in the charging mode, we derive a similar model for the discharging case.

B. Second Case: Discharging Mode

To modify the charging model in Fig.3 for the discharging mode two slight changes are required: *i)* changing the firing angle to $\beta = \pi - \alpha$; and *ii)* changing the current flow direction. Therefore, the obtained battery voltage is

$$V_{BT} = V_{BOC} - V_{B1} - (R_{BT} + V_{BS}) I_{BES} \tag{40}$$

Considering the inverse flow of the current, I_{BES} has negative value in the equation (14). So, (40) can be modified to

$$V_{BT} = V_{BOC} - V_{B1} + (R_{BT} + V_{BS}) I_{BES} \tag{41}$$

IV. Simulation Results

To validate the credibility of the obtained linearized model in *d-q* axes, simulations were conducted to compare the behavior against the original model. For brevity, only the results for the charging mode are discussed. The discharging mode has the same quality of results. In the simulation study, the following system operating conditions were considered: $v_{tq0} = 100\ V$, $v_{td0} = 692.82\ V$, $v_{t0} = 700\ V$, and $\alpha_0 = 15°$.

At this operating point, a small perturbation on the firing angle of the inverter with the value of $\Delta\alpha = -1.97°$ was considered. Figure 4 compares the results of the state vector $x_b = [V_{BOC}, V_{Bq}, \alpha_R]^T$ in both models. The states in the original model are shown in blue and states of the linearized *d-q* axis model are depicted with red.

All states start with the same initial conditions as both models were in the same operating points. The slopes of deviations are very close to each other and there are slight differences in the final values.

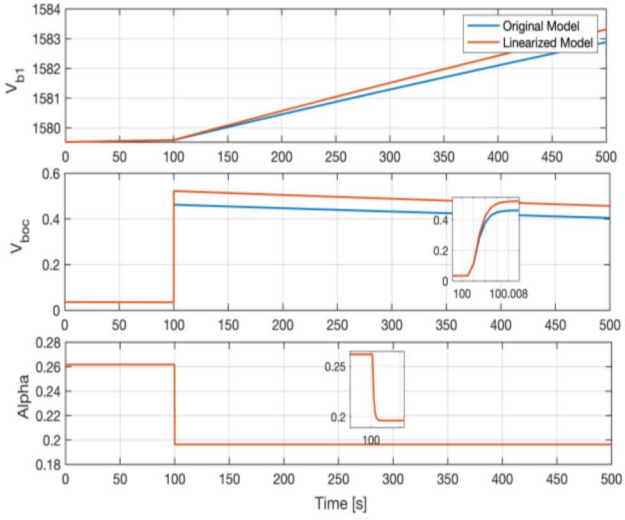

Fig. 4. Open circuit voltage of the battery

The bias errors are mainly noticeable in the steady state because of the linearization approximation whereas the application of this model is for transient behavior in small signal analysis for no more than a few minutes time duration. In the original model depicted in Fig. 3, there is no direct access to measure the *d-q* axis currents of the battery. Therefore, to validate the output signals of the obtained model, we compute these currents by solving the following equations for active and reactive power, which approximates (20)-(24) as

$$P_{BES} = v_{td} I_{bd} + v_{tq} I_{bq} \tag{42}$$

and

$$Q_{BES} = v_{td} I_{bq} - v_{tq} I_{bd} \tag{43}$$

The battery current in *d* and *q* axes (I_{bd}, and I_{bq}) of the original model and the linearized model are shown in Fig. 5. The linearized model results are close to the original model, particularly in the transient time frame that would be employed in small signal stability studies.

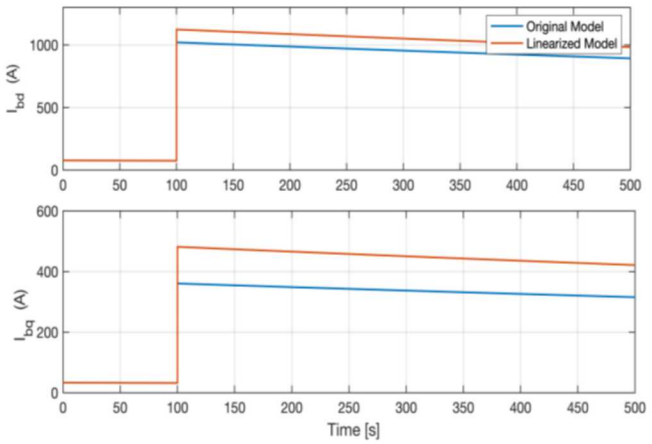

Fig. 5. Battery *d* axis output current

V. Conclusion

In this paper an analytical linearized dynamic model of a large-scale BESS in the *d-q* axes is presented. The model is expressed in the state space representation which can be easily applied in stability studies and applications in the power system. The lack of a parametric based model of BES in *d-q* axes makes stability analysis challenging especially when the contributions of batteries are growing rapidly in power systems. To examine the dynamic behavior of this model, the active and reactive power of the linearized model are compared to those of the original model. Battery integration to the power grid improve the stability and transient behavior of the system. Considering the firing angle deviation as an input for the battery model allows us to control the output power of the battery along with its power factor. For future work, we will evaluate the effects of the battery integration on the power system. Also, the impact of the power factor deviation as a control input on the small signal stability of the power system will be studied to improve the small signal stability of the system.

ACKNOWLEDGEMENT

The authors gratefully acknowledge financial support from the U.S. Department of Energy's Energy Storage Program, managed by Dr. Imre Gyuk. Sandia National Laboratories is a multi-mission laboratory managed and operated by National Technology and Engineering Solutions of Sandia, LLC., a wholly owned subsidiary of Honeywell International, Inc., for the U.S. Department of Energy's National Nuclear Security Administration under contract DE-NA0003525.

Appendix

System parameters are:

$X_{co} = 0.0274\ \Omega,\quad C_{BP} = 52600\ F,\quad C_{B1} = 1\ F,\quad R_{BT} = 0.0167\ \Omega, R_{BS} = 0.013\ \Omega, R_{B1} = 0.001\ \Omega, R_{BP} = 10000\ \Omega, K_R = 1, T_R = 0.001\ s, v_{t0} = 790\ V, v_{q0} = 100\ V, \alpha = 15°.$

References

[1] Lu, Chun-Feng, Chun-Chang Liu, and Chi-Jui Wu. "Effect of battery energy storage system on load frequency control considering governor deadband and generation rate constraint." *IEEE Transactions on Energy Conversion* 10.3 (1995): 555-561.

[2] S. Kalyani, S. Nagalakshmi, R. Marisha, "Load frequency control using battery energy storage system in interconnected power system," Third International Conference on Computing Communication & Networking Technologies (ICCCNT), 2012, pp 1-6.

[3] Liang Liang, J.Zhong, Z.Jiao, "Frequency regulation for a power system with wind power and battery energy storage," IEEE International Conference on Power System Technology (POWERCON), 2012, pp1-6.

[4] S. K. Aditya, and D. Das. "Application of battery energy storage system to load frequency control of an isolated power system." *International journal of energy research* 23.3 (1999): 247-258.

[5] S. Ervin, G. Balzer, and A. Danesh Shakib. "The Impact of the" Wind Farm-Battery" Unit on the Power System Stability and Control." *2007 IEEE Lausanne Power Tech*. IEEE, 2007.

[6] Chandra, Souvik, Dennice F. Gayme, and Aranya Chakrabortty. "Using battery management systems to augment inter-area oscillation control in wind-integrated power systems." *2013 American Control Conference*. IEEE, 2013.

[7] Datta, Ujjwal, Akhtar Kalam, and Juan Shi. "Battery energy storage system for transient frequency stability enhancement of a large-scale power system." *2017 Australasian Universities Power Engineering Conference (AUPEC)*. IEEE, 2017.

[8] Beck, J. W., Carroll, D. P., Gareis, G. E., Krause, P. C., & Ong, C. M. (1976). A computer study of battery energy storage and power conversion equipment operation. IEEE Transactions on Power Apparatus and Systems, 95(4), 1064-1072.

[9] Salameh, Ziyad M., Margaret A. Casacca, and William A. Lynch. "A mathematical model for lead-acid batteries." IEEE Transactions on Energy Conversion 7.1 (1992): 93-98.

[10] Lu, C-F., C-C. Liu, and C-J. Wu. "Dynamic modelling of battery energy storage system and application to power system stability." IEE Proceedings-Generation, Transmission and Distribution 142.4 (1995): 429-435.

[11] Adrees, Atia, Hooman Andami, and Jovica V. Milanović. "Comparison of dynamic models of battery energy storage for frequency regulation in power system." 2016 18th Mediterranean Electrotechnical Conference (MELECON). IEEE, 2016.

[12] Padyar, K. R. "Power System Dynamics Stability and Control, Hyderabad, AP." (2002).

[13] Shubhanga K. N. "Power System Analysis, a dynamic presentation" Pearson, 2018